JOURNAL OF GEOPHYSICAL RESEARCH, VOL. 111, C10016, doi:10.1029/2005JC002905, 2006

Synoptic maps of temperature and velocity within the Subantarctic Front south of Australia

K. L. Tracey,[1] D. R. Watts,[1] C. S. Meinen,[2] and D. S. Luther[3]

Received 4 February 2005; revised 13 April 2006; accepted 19 June 2006; published 28 October 2006.

[1] From April 1995 to March 1997 a 450-km array of inverted echo sounders, horizontal electric field recorders, and current meters measured the horizontal and vertical structure of the current, temperature, and salinity fields associated with the Subantarctic Front (SAF) south of Australia. Synoptic maps of the temperature and velocity fields often show the SAF divided into two zonally separated jets, which are also found in the mean. These jets were in close proximity yet directed toward different azimuths. The daily maps also show that the SAF often flowed as a single strong jet, during which times it underwent vigorous meandering, with crest-to-trough meridional distances ~250 km. These meanders stalled within the array and contorted to form "S"-shaped paths. In one case a cold-core ring was formed. Propagating meanders have periods of 20–70 days, wavelengths of 240–420 km, and phase speeds of 12–6 km d^{-1}. Deep currents reveal strong cyclones and anticyclones propagating primarily eastward through the array beneath the meandering jet. Thus, at times the deep flow is aligned with the upper flow, whereas at other times, significant barotropic flows cross the upper front. Occasionally, the northern Polar Front was also found within the array. The observed variability illustrates how the interaction of a meandering current with transient features such as meanders and eddies makes the identification of a front difficult when a single isotherm or isopycnal is utilized as the definition.

Citation: Tracey, K. L., D. R. Watts, C. S. Meinen, and D. S. Luther (2006), Synoptic maps of temperature and velocity within the Subantarctic Front south of Australia, *J. Geophys. Res.*, *111*, C10016, doi:10.1029/2005JC002905.

1. Introduction

[2] The Antarctic Circumpolar Current (ACC) is a broad region of strong eastward flow encircling the entire Southern Ocean. It consists of several fronts, of which the Subantarctic Front (SAF) and the Polar Front (PF) are the two strongest branches. The SAF is typically identified by the strong temperature gradient between 4°–8°C at 400 dbar and the PF by the northernmost extent of 2°C at 200 dbar. *Rintoul et al.* [2001] review the ACC system, and *Belkin and Gordon* [1996] and *Orsi et al.* [1995] discuss the properties of the Southern Ocean fronts.

[3] Prior to 1995 empirical knowledge of the SAF had come from a limited number of hydrographic studies as well as a few moored experiments [*Bryden and Heath*, 1985; *Whitworth and Nowlin*, 1987], from analyses of surface drift currents [*Patterson*, 1985; *Johnson*, 1989], and from satellite sea surface temperature and sea surface height studies [*Chelton et al.*, 1990; *Mestas-Nunez et al.*, 1992; *Gille*, 1994; *Morrow et al.*, 1994; *Park and Gamberoni*, 1995]. Each of these studies advanced our understanding of the ACC system, however their limitations included either low horizontal resolution, short temporal duration, or limited vertical coverage.

[4] In particular, south of Australia, the majority of historical observations of the SAF are from hydrographic sections. In this region, the SAF is usually located between 50°S and 52°S and a thermostad of Subantarctic Mode Water is located just to the north of the front. Hydrographic data collected prior to 1990 are summarized in a global Southern Ocean study by *Orsi et al.* [1995]. After 1990, most sections have been taken as part of the World Ocean Circulation Experiment (WOCE) project [e.g., *Rintoul and Sokolov*, 2001]. One result of these sections has been to confirm the zonation of the ACC, and to suggest that the two strong branches of the ACC may themselves be broken into multiple branches [*Belkin and Gordon*, 1996; *Sokolov and Rintoul*, 2002]. The sections have also provided snapshot estimates of the transport of the SAF. Generally these estimates have been of only the baroclinic component of the transport, although one study in the Pacific sector east of Australia used acoustic Doppler current profiler data to get absolute velocities with accuracies of roughly 3 cm s^{-1} [*Donohue et al.*, 2001].

[5] The first moored study of the SAF south of Australia (AUSSAF) was a 2-year experiment during 1993–1995. *Phillips and Rintoul* [2000, 2002] investigated the SAF

[1]Graduate School Of Oceanography, University of Rhode Island, Narragansett, Rhode Island, USA.
[2]Atlantic Oceanographic and Meteorological Laboratory, NOAA, Miami, Florida, USA.
[3]School of Ocean and Earth Science and Technology, Department of Oceanography, University of Hawai'i at Manoa, Honolulu, Hawaii, USA.

0148-0227/06/2005JC002905$09.00

using current meter data on four moorings near 51°S, 143.5°E, where they found the mean flow was toward the northeast. This had not been noticed previously in coarser-resolution hydrographic [e.g., *Reid*, 1997] data sets, which show the front oriented east–west or ESE–WNW, but had been suggested by the analyses of altimetric observations [*Gille*, 1994]. Instantaneously, the current data showed that the SAF flowed as a meandering jet with energetic coherent fluctuations at periods from 2 to 90 days, with a dominant period near 20 days, and with speeds 30 cm s^{-1} even down to 1150 dbar.

[6] Soon after, in March 1995, a more extensive and comprehensive observational program, titled "Sub-Antarctic Flux and Dynamics Experiment" (SAFDE) [*Luther et al.*, 1997], was initiated. The program was a collaboration between U.S. and Australian scientists. The objective was to observe the structure and variability of the absolute (barotropic and baroclinic) current and temperature fields within the Subantarctic Front south of Tasmania using a long-duration, spatially coherent moored array. The suite of instruments deployed incorporated both well established oceanographic tools (an array of current meter moorings), as well as novel approaches (an array of horizontal electric field recorders and inverted echo sounders). These seafloor instruments are well suited for observing currents like the ACC where large vertical scales dominate.

[7] SAFDE yielded a data set that is unique in both its spatial and temporal extent in the Southern Ocean. The mesoscale-resolving array provided observations of the horizontal and vertical structures of temperature, salinity, velocity and stream function [*Watts et al.*, 2001] which were mapped on a daily basis for a 2-year period. These daily maps can be used to visualize the density and flow fields in this complex current regime.

[8] The purpose of this paper is to utilize the mapping capabilities of the SADFE array to illustrate the variety of configurations the SAF can exhibit in this region. In the mean, the maps of temperature and velocity show two jets separated by a region with weaker gradients. The temporal evolution of the SAF is illustrated for four circumstances: (1) two relatively stable jets, (2) vigorous meandering of a single jet, (3) formation of a cold core eddy, and (4) propagation of a small-amplitude meander. Daily maps of the deep stream function reveal cyclones and anticyclones propagating through the region similar to those observed beneath the Gulf Stream [*Watts et al.*, 1995; *Shay et al.*, 1995; *Savidge and Bane*, 1999]. The deep currents are directed around these low- and high-pressure anomalies rather than aligned with the upper front, often resulting in significant cross-frontal and vertical motions, as was observed in the Gulf Stream [*Lindstrom et al.*, 1997]. The 4-year-long velocity records measured during AUSSAF and SAFDE alternate between intervals (several months in length) of weak and strong fluctuations, suggesting a possible quasi-biennial oscillation in the variability of the SAF.

2. Data

[9] The complete SAFDE array spanned a 450 km distance between Tasmania and Antarctica and comprised 18 inverted echo sounders (IESs), 17 horizontal electric field recorders (HEFRs), and 9 current meter moorings (RCMs). Most of the instruments were concentrated in a central region near 50°S (Figure 1). The SAFDE array was oriented along a SSW–NNE line overlapping the WOCE SR3 repeat hydrography track that was approximately perpendicular to the mean axis of the SAF, indicated by dynamic height contours in Figure 1. The instruments were deployed for a 2-year period beginning in April 1995.

[10] A novel aspect of SAFDE was the deployment of a suite of IESs and HEFRs to estimate time series of the vertical profiles of velocity, temperature, and dynamic height. The IESs were spaced 30 km apart along two parallel lines spanning a north–south distance of about 270 km and separated zonally by 55 km. The IESs measure acoustic travel time from the seafloor to the surface and back. Using the hydrographic measurements taken along the SR3 track by S. Rintoul and his collaborators together with CTD casts taken on the SAFDE deployment and recovery cruises, characteristic relationships between travel time and temperature and specific volume anomaly were developed. These were combined with the IES travel time measurements to estimate full water column profiles of temperature and specific volume anomaly following the methods developed by *Meinen and Watts* [2000]. The profiles of specific volume anomaly were vertically integrated to produce profiles of dynamic height from the IES measurements. *Watts et al.* [2001] demonstrate the effectiveness of this technique for the SAF region in that at least 95% of the variance of the temperature and specific volume in the thermocline region is captured.

[11] The HEFRs were positioned about 30 km apart along a line located midway between the two IES lines (Figure 1). The HEFRs measure the horizontal electric fields which are related to the conductivity-weighted, vertically averaged currents [*Sanford*, 1971; *Chave and Luther*, 1990; *Luther et al.*, 1991]. Unfortunately, the compasses of all the HEFRs yielded inaccurate directions because of the extreme inclination (>75°) of the Earth's magnetic field in the region. In addition, the amplitudes of the horizontal electric field varied significantly (up to 40%) between sites. It was determined that these amplitude differences were not instrumental, but were caused by galvanic distortion of the electric field due to lateral gradients in electrical conductivity caused by the rough topography [*Chave et al.*, 2004]. *Chave et al.* [2004] discuss these problems and their solutions which utilize the highly polarized, highly coherent, high-frequency (>4 cpd) electric field signals originating in the ionosphere to align and scale the data.

[12] Corrections due to the vertical structure of conductivity (±1–4%) were directly estimated from the IES data and applied to the HEFR measurements to yield vertically averaged water velocity ($\mathbf{V}_{VA}$). *Meinen et al.* [2002] estimate that after all the corrections have been applied the daily HEFR $\mathbf{V}_{VA}$ currents have an accuracy of ±3 cm s^{-1}.

[13] Horizontal gradients of dynamic height between adjacent IES sites can be used to determine profiles of velocity normal to the measured gradients and relative to the bottom using the geostrophic method [*Kim and Watts*, 1994; *He et al.*, 1998]. The two-dimensional IES array provided measurements of both the zonal and meridional gradients, thus resolving both velocity components. Furthermore, the IESs were positioned to surround seven of the HEFR sites

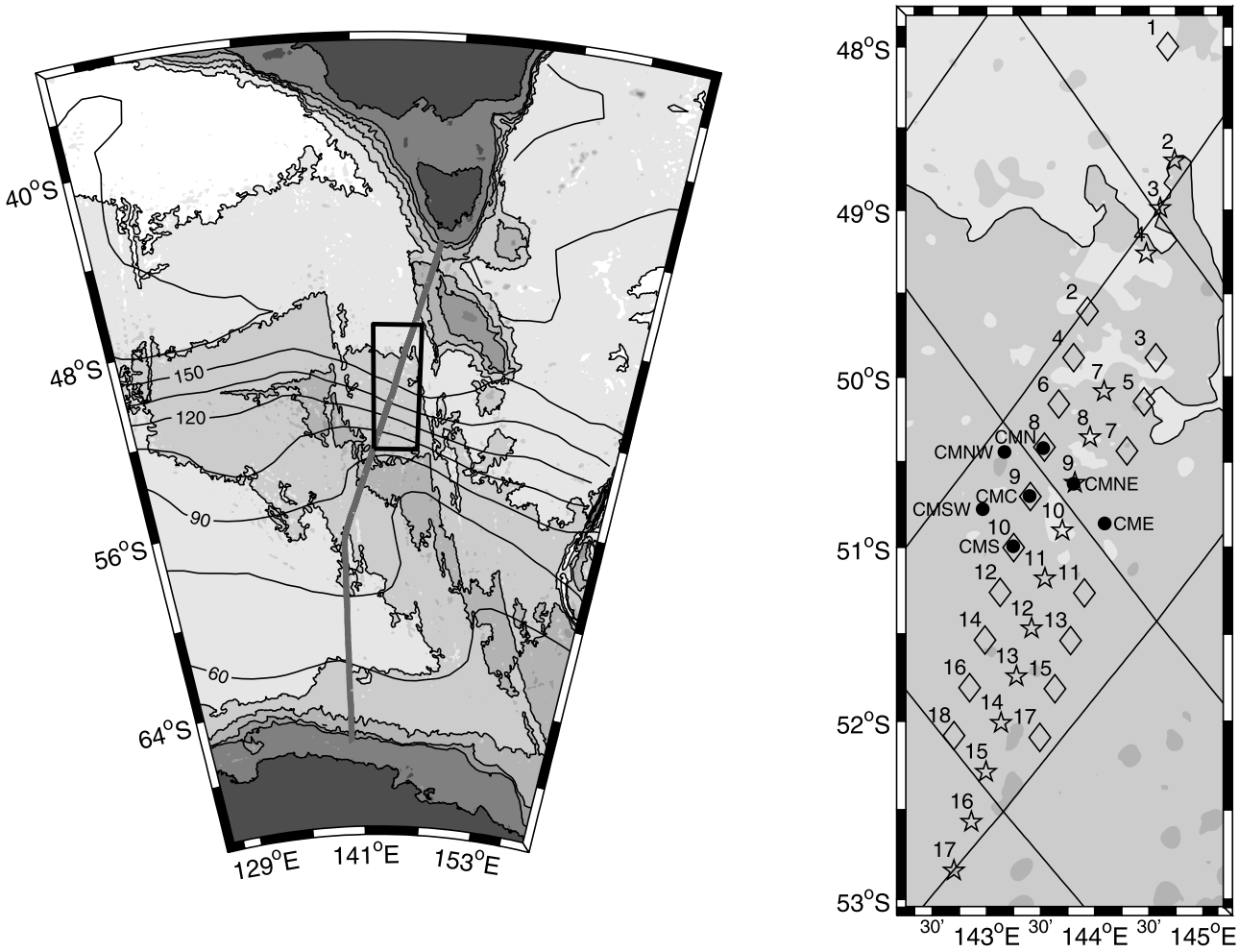

Figure 1. SAFDE array. IESs are shown by open diamonds, HEFRs by open stars, and RCM moorings by solid circles. IES and HEFR sites are labeled to the upper left; RCM labels are shifted for clarity. The box in the left frame outlines the region that is enlarged at the right. Bottom topography [*Smith and Sandwell*, 1997] is gray shaded every 1000 dbar, with darker shades indicating shallower depths. The bold gray line shows the WOCE SR3 line which coincides with the western line of IESs. Dynamic height at 200 m relative to 2000 m (dyn cm) from the 1° × 1° gridded data set of *Olbers et al.* [1992] is contoured. TOPEX/Poseidon ground tracks are shown.

so that their relative velocity profiles could be combined with the $\mathbf{V}_{VA}$ from those HEFRs to yield vertical profiles of absolute velocity (u_p, v_p) as a function of time. *Meinen et al.* [2002] provide a full description of this technique.

[14] At the center of the SAFDE array, nine nearly full-depth moorings were deployed as a local dynamics array (LDA). Of these, four complete moorings and three partial moorings were recovered in March 1997. Three of the complete moorings were situated along the SR3 track and were at the same locations as three of the previous AUSSAF moorings [*Phillips and Rintoul*, 2000, 2002]. The fourth complete mooring was located along the eastern line of IESs. The three partial moorings yielded 2000 m current and temperature records at two sites to the west of the SR3 line and at one site that was collocated with a HEFR site. The data recovered from some of the upper level current meters were compromised by faulty compasses and pressure sensors. Therefore, only the current measurements at 2000 m were complete enough to map the stream function (ψ_{2000}) within the LDA. (The regional average ψ_{2000} is assumed zero for each daily map.) It was not necessary to correct these deep measurements for mooring motion as is typically done for shallower current meters.

[15] All data were low-pass filtered using an eighth-order Butterworth filter (fourth-order passed both forward and backward to eliminate phase shifting) with a 72-hour cutoff period. All spectra were computed using a modified Welch method, where the records were broken into 256-day segments with 50% overlap and scaled with a Hamming window. The spectral estimates are plotted in variance-preserving form in the next section.

[16] Horizontal maps of temperature at 400 dbar (T_{400}) were produced from the IESs following objective mapping techniques of *Bretherton et al.* [1976] using the modifications discussed by *Tracey et al.* [1997] with correlation functions and averaging periods suited to these data. To fill one gap between IESs along the eastern line, the temperature and pressure records from the RCMs at 4 levels at

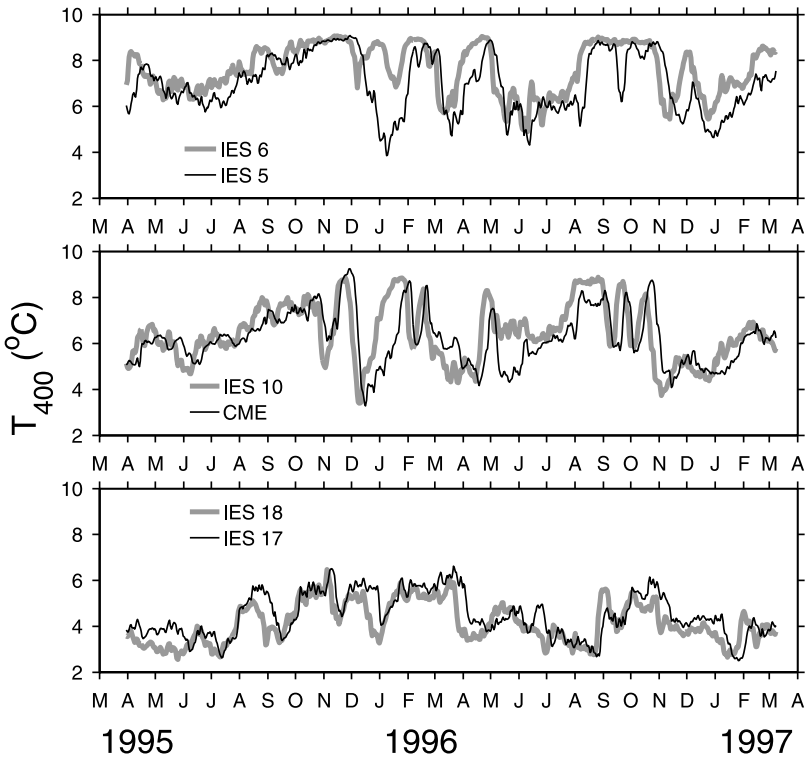

Figure 2. Temperature at 400 dbar at five IES sites and at site CME which was treated as a pseudo-IES. Each pair of sites is separated zonally, and the phase lag between their temperature records arises from generally eastward propagation of features.

mooring site CME were used to create a "pseudo-IES" travel time record following the method presented by *Meinen and Watts* [2000]. This pseudo-IES record was used to produce temperature and specific volume anomaly profiles in the same manner as the real IES records. The pseudo-IES data were included in the mapping procedure in order to better resolve the meridional temperature gradients in that region of the mapped fields.

[17] Sea surface height (SSH) maps are used to provide an expanded view of the ACC fronts in the region surrounding the SAFDE array. The SSH anomaly fields are the delayed time, merged product distributed by AVISO. The altimetry data have been objectively mapped onto a one-third degree regular grid at 7-day intervals for the 1995–1997 time period. To produce absolute SSH maps, we added the Rio03 mean steric height (relative to 1500 m depth) produced by CLS Space Oceanography Division and described by *Rio and Hernandez* [2004]. This mean was chosen because the features in resulting SSH maps resembled those resolved by the SAFDE measurements most closely among the means we examined.

3. Temporal Variability

[18] Time series of temperature and velocity will be shown for several sites to illustrate the variability of the flow in the SAFDE array. The illustrated sites were chosen to span the north–south range of the array. The fluctuations at these sites differ because of differences in their locations relative to the mean SAF front.

[19] Temperatures at 400 dbar for six IES sites are shown in three panels (Figure 2). Each panel displays the T_{400} records of a pair of IESs located at approximately the same latitude on the western and eastern lines. Temperature fluctuations in the northern and central portions of the array (upper two panels) are nearly twice as large as those at the southern end. These large fluctuations (on the order of 4°C) occur as the SAF shifts laterally across the northern half of the array. Events occurring along the eastern line lag those at the western line. Covariances calculated for all three pairs of IES were maximized when the data from the eastern line were shifted by 6–8 days. Given the 55 km distance separating the two lines, this time lag yields an average eastward propagation speed of 6–9 km d^{-1}. The coherences of these pairs of records were calculated and the corresponding phase lags were used to determine phase speeds and wavelengths of the coherent frequencies. Meanders with periods of 20–70 days had wavelengths of 240–420 km and phase speeds of 12 km d^{-1} to 6 km d^{-1}. These wavelengths are 1.5–2 times larger than the wavelengths yielding maximum growth rates for baroclinic instability in the region in the FRAM and POP numerical models [*Best et al.*, 1999].

[20] The combined HEFR and IES measurements yield full-depth water column profiles of absolute velocity. Zonal (u_p, positive eastward) and meridional (v_p, positive northward) velocities at four of the levels (0, 400, 2000, and 3500 dbar) are illustrated in Figures 3a, 3b, and 3c for three sites. A distinctive feature of the velocities at northern (HEFR 7) and middle (HEFR 11) sites is the change in character of the records during the 2-year measurement period. During the initial 6 months (April–October 1995) both velocity components are relatively steady (standard deviations 8–10 cm s^{-1}). In contrast, during the next

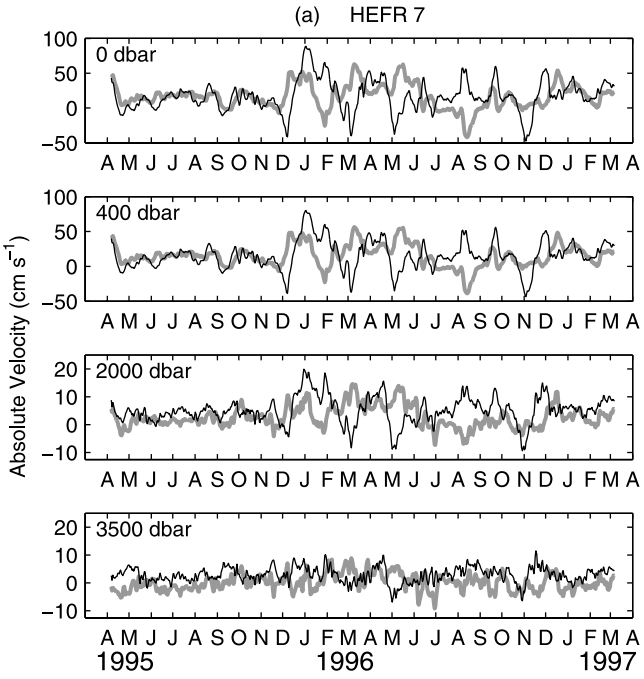

Figure 3a. Zonal (u, thick gray lines) and meridional (v, thin black lines) absolutely referenced velocity derived from the combined IES and HEFR measurements. Velocities are shown at four levels at HEFR 7. The ranges of the ordinate differ by level.

6 months (December 1995 to May 1996), large fluctuations (standard deviations 16–35 cm s^{-1}) are observed at periods of 1–2 months. The variability remained high during the second year of deployment. At HEFR 14, at the southern end of the mapping array, the variability was fairly uniform throughout the 2-year period.The currents at HEFR 7, 8, and 9 were highly coherent with one another. Likewise, the currents at HEFR 13 and 14 were also coherent. However, the coherence between these two groups was weak.

[21] At all three locations, the currents are correlated from the surface down to 2000 dbar (Figures 3a, 3b and 3c). This high vertical correlation is in agreement with the previous current observations in this region of *Phillips and Rintoul* [2000] and has been reported at other locations along the ACC [e.g., *Sciremammano et al.*, 1980; *Bryden and Heath*, 1985]. Hydrographic sections conducted in this region [cf. *Rintoul and Bullister*, 1999] also show that the baroclinic signature of the fronts extends from the sea surface down to the seafloor. The cross-correlations between the 400 dbar and 2000 dbar currents exceed 0.9 with little or no time lag. The baroclinic flow weakens with depth such that the higher-frequency barotropic abyssal currents dominate the deeper records. Cross-correlations between the 400 dbar and 3500 dbar currents are maximized (values of 0.35–0.7) at time lags of 5–10 days with the deep features leading the upper.

[22] Variance-preserving spectra are shown for the 400, 2000 and 3500 dbar levels (Figure 4). Regardless of location, all spectra for the 400 dbar level exhibit a broad spectral peak between 25–125 days and minimal energy at periods shorter than 10 days. Although these data have been low-pass filtered to remove the signals shorter than 3 days, the unfiltered velocities measured by current meters (0.5 hour sampling interval) exhibited prominent spectral peaks at only the semidiurnal tidal and inertial periods. The spectra for HEFR 11 are similar to those reported by *Phillips and Rintoul* [2000] from a current meter moored at 2240 dbar at a nearby location. Additionally, the spectra for the 2000 m velocities at HEFR 9 (not shown) and those obtained for velocities directly measured by a current meter collocated at the site during SAFDE both show nearly the same peak variance at 50 days. The good agreement between these independent estimates indicates that the HEFR + IES methodology reproduces the velocity variability well (see *Meinen et al.* [2002] for more details).

4. Eulerian Mean and Standard Deviations

[23] Time averages of the T_{400} and ψ_{2000} fields are presented in Figure 5. The temperature contours shown in the following figures map the baroclinic flow at 400 dbar, and throughout the text the terms "front" and "jet" are used interchangeably. Along the western IES line, the mean temperatures range from 8°C in the northern corner to 4°C at the southern edge, indicating that in the mean the SAF was centered in the array. Eastward of this line the isotherms fan out resulting in a weaker meridional temperature gradient (only a 3°C range in the mean) along the eastern line. Although the orientation of the SAFDE array and SR3 line were approximately perpendicular to the historical mean direction of the front determined by *Olbers et al.* [1992] and shown in Figure 1, in fact, the observed mean path for the 2-year experiment crosses the array obliquely. The waters warmer than 6°C generally flow

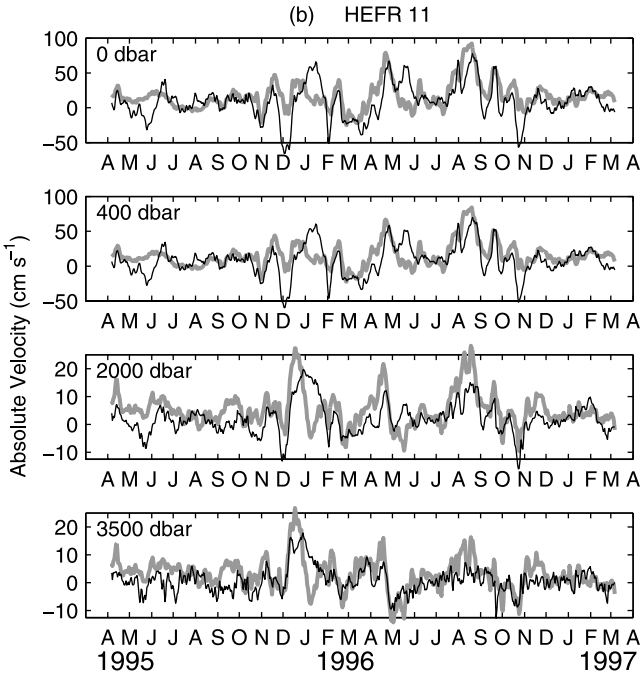

Figure 3b. Zonal (u, thick gray lines) and meridional (v, thin black lines) absolutely referenced velocity derived from the combined IES and HEFR measurements. Velocities are shown at four levels at HEFR 11. The ranges of the ordinate differ by level.

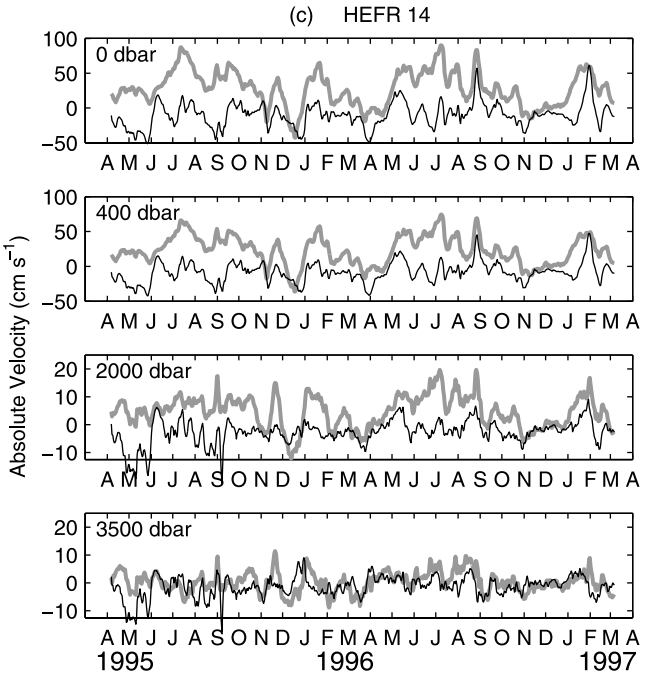

Figure 3c. Zonal (u, thick gray lines) and meridional (v, thin black lines) absolutely referenced velocity derived from the combined IES and HEFR measurements. Velocities are shown at four levels at HEFR 14. The ranges of the ordinate differ by level.

toward the northeast (heading 050–055°T), nearly 60° more to the north than expected. This direction is consistent with the northeastward mean flow reported by *Phillips and Rintoul* [2000] from current meters in a preceding experiment at this same location and with the stream coordinate analysis of the SAF structure using the SAFDE data [*Meinen et al.*, 2003]. The cooler waters (4°–5°C) flow in a different direction, heading slightly south of east, which is more aligned with the historical mean path. Mean current speeds at 400 dbar in both jets are 28–32 cm s^{-1}.

[24] The mean currents and their standard deviation ellipses are shown in Figure 6. Mean vectors which are larger than their respective ellipses indicate that the daily currents are relatively stable, while the vectors contained within the ellipses indicate no prevalent current direction. Nearly all the means are significant, however, because the standard error of the mean is reduced from the daily standard deviation by $\sqrt{N}$, where N is the ratio of the sample length to the integral time scale. Using the longest ellipses in Figure 6 at 400, 2000, and 3500 dbar, the estimated error of the mean is less than 4.5 cm s^{-1}, 1.5 cm s^{-1}, and 1.0 cm s^{-1}, respectively. The mean vectors and the ellipses turn about the vertical in a consistent pattern across the array. The rotation is cyclonic with decreasing depth (backing) at the northern sites indicating downwelling of cold waters toward the equator. At HEFR 14, a southern site, the rotation is anticyclonic (veering) indicating upwelling of warm waters poleward. The southern mean flow roughly parallels the bathymetry, and it turns (veers) very weakly across the sloping isotherms. The mean northern flow crosses northward down the bathymetry and turns (backs) notably across and down the more steeply sloped isotherms, which imparts a vertical stretching to the lower water column. The sign of this vertical stretching (negative $\partial w/\partial z$) is consistent with the observed mean horizontal divergence of the two fronts.

[25] The mean deep stream function at 2000 m (Figure 5) shows higher pressure in the northwest corner and lower pressure in the southeast corner. Between these two regions, the streamlines trend toward the northeast nearly aligned with the upper T_{400} front. This pattern suggests that on average the RCMs on the western side typically sampled the southern (anticyclonic) portion of a high-pressure anomaly and those on the eastern side measured the northern

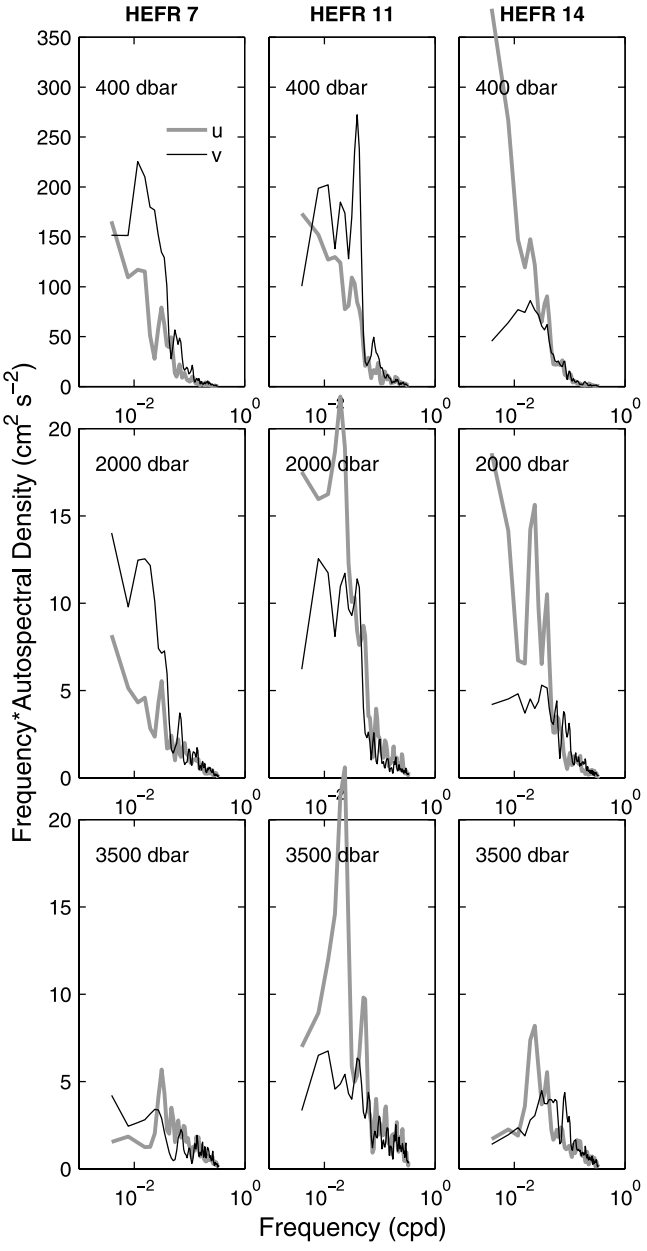

Figure 4. Variance-preserving spectra for the 400, 2000, and 3500 dbar level currents at the indicated HEFR locations. The u and v components are denoted in the key in the top left panel. The ranges of the ordinate vary by level.

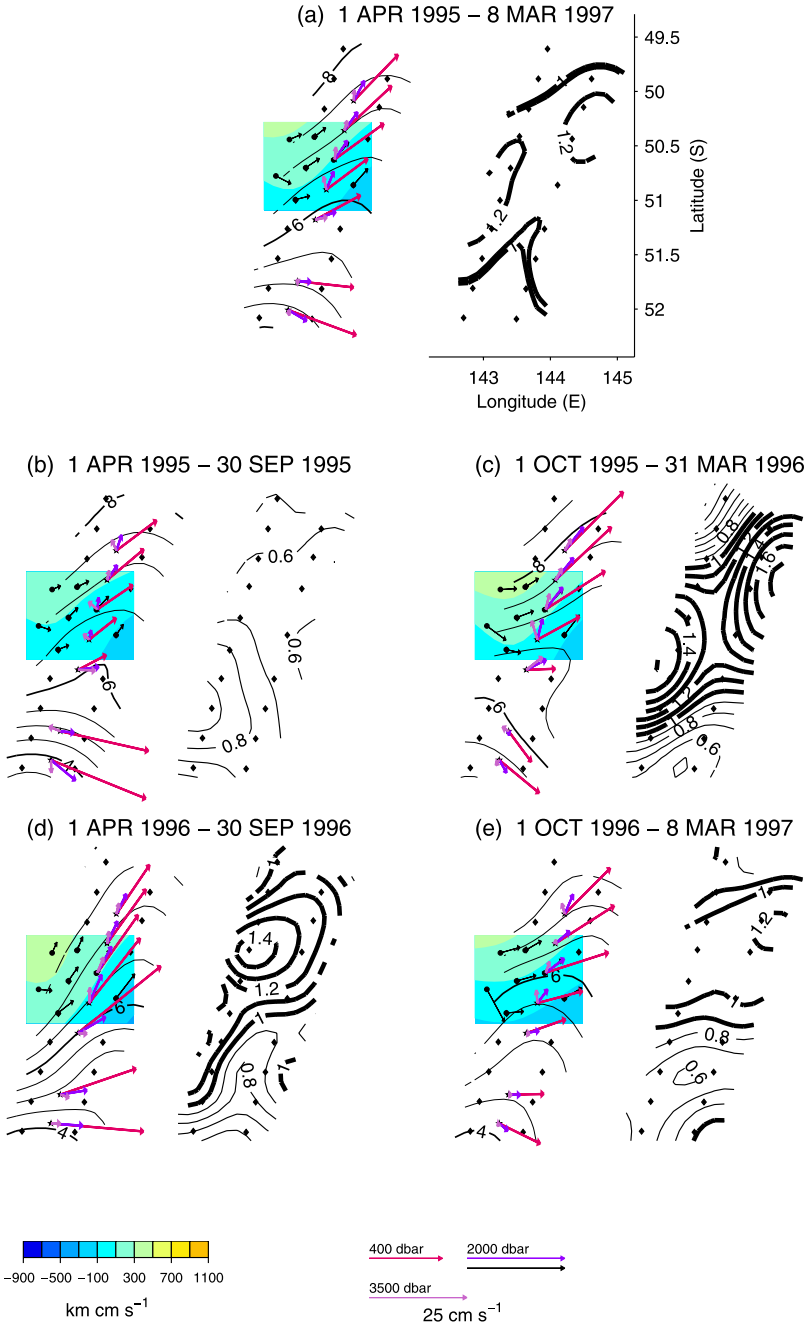

Figure 5. Mean and standard deviation fields for (a) the 2-year period spanning 1 April 1995 to 8 March 1997 and (b)–(e) four 6-month-long averaging periods. (left) Mean temperature at 400 dbar, T_{400} (thin and bold solid contours, 0.5°C intervals) and stream function field at 2000 dbar, ψ_{2000} (color-coded, 200 km cm s^{-1} interval) in plan view. Black vectors show the measured currents used to produce the ψ_{2000} fields. Mean velocities at 400, 2000, and 3500 dbar measured by the HEFR + IES are plotted in color. Vector scales vary by level (see key). (right) Standard deviation of the T_{400} field (contour interval of 0.1°C). The small solid symbols indicate the IES, HEFR, and RCM sites shown in Figure 1.

(cyclonic) portion of a low-pressure anomaly. It should be noted that even as deep as 2000 m the baroclinic shear contributes substantially to the flow (see Figures 3a, 3b and 3c). The mean speeds at 2000 dbar are 6–8 cm s^{-1} while those at 3500 dbar are only slightly smaller (4–6 cm s^{-1}).

[26] The temporal variability at each grid point is quantified by the standard deviation fields (Figure 5). The standard deviation of T_{400} exceeds 1°C nearly everywhere within the array. A ridge of high standard deviation, approximately 60 km wide, trends to the northeast under the steepest portion of the mean temperature front. The high standard deviations arise from the diversity of pathways observed during the averaging period. Lower standard deviations occurred at the northern and southern edges of the mapping array. The low variability to the north is consistent with the presence of a thick thermostad

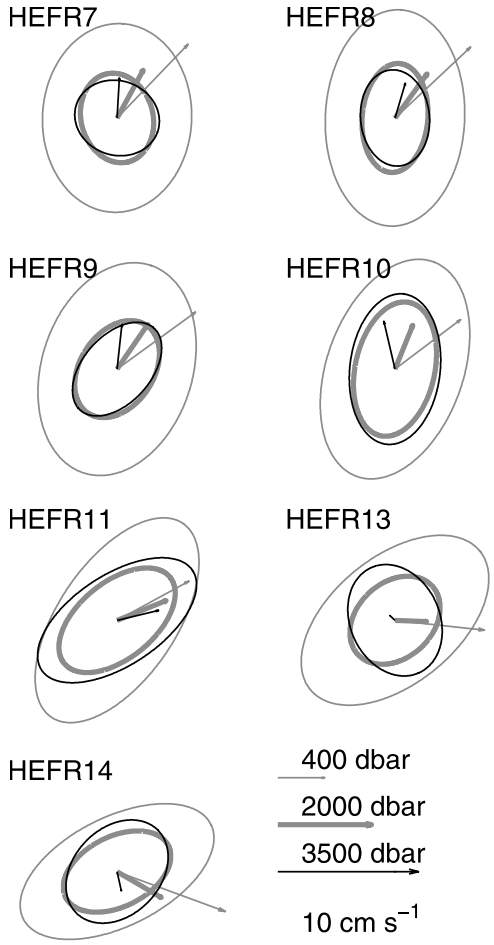

Figure 6. Mean currents and their standard deviation ellipses at 400 dbar (thin gray), 2000 dbar (thick gray), and 3500 dbar (black). Scales vary by level (see key).

of Subantarctic Mode Water with temperatures near 9°C [*Rintoul and Bullister*, 1999].

[27] To examine the stability of the mean fields, the T_{400} and ψ_{2000} fields were divided into 6-month-long subsets prior to averaging. The April–September and October–March intervals were chosen in order to use the complete set of observations. The subset encompassing the final portion of the observational period was 163 d, slightly shorter than 6 months. The resulting mean and standard deviation fields for the four subsets are shown in Figure 5. All four mean fields show the region crossed by two fronts, although the strengths and orientations of the fronts differ between them. For example, during the final 6-month period (Figure 5e) the meridional T_{400} gradients were relatively uniform and only weakly separated into two fronts.

[28] In the LDA, the orientation of the high- and low-pressure anomalies in the ψ_{2000} fields are quite similar for all 6-month-long averaging periods. The diagonally offset pressure cells result in northeastward mean flow occurring at most of the mooring sites. The notable exception is the westernmost RCM where the mean flow was directed southeastward.

[29] While the 6-month mean fields are similar, the T_{400} standard deviation fields are strikingly different. During the first 6-month period, April–September 1995, the standard deviations were considerably smaller (ranging 0.5°–0.8°C) than all the other periods, indicating that little meandering occurred. In contrast, the largest standard deviations (peak values exceeding 1.6°C) were observed during the next 6-month period, October 1995 to March 1996, which was the period of greatest meandering. During October 1996 to March 1997, high standard deviations were confined to the northern portion of the array, signifying that the northern part of the SAF front translated southward infrequently.

5. Case Studies

5.1. Two Persistent Fronts

[30] Figure 7 presents a series of individual maps for a 2.5-month period from the relatively inactive first 6 months. Adjacent frames beginning in June 1995 reveal a slowly evolving T_{400} field with two frontal regions, each meandering individually. On 18 June, the SAF exists as a single coherent jet at the western IES line. Yet at the eastern IES line the flow is separated into two jets. Over the course of a month, the branching takes place increasingly farther to the west such that by 12 July the flow is divided into two branches.

[31] The SSH fields for this time period show a broader view of the fronts in this region (Figure 8a). Three height contours are emphasized to indicate the approximate paths of the two SAF fronts and the northern Polar Front. The contours were identified by comparison with the moored data where they passed through the array. The SSH fields for early June 1995 show two distinct fronts to the west that were brought together by a large meander crest immediately northwest of the array. The SSH field for 21 June (Figure 8a) agrees that the merged branches reseparate at the eastern edge of the array, and shows that another large meander formed downstream in the northern branch.

[32] This two-front configuration was observed on four occasions during the 2-year experiment, each persisting for 1–2 months. The evolution of current and temperature fronts during this 2-month period in 1995 is characteristic of all four occurrences:

[33] 1. The northern jet typically carries water warmer than 7°C to the northeast. This front passes over the LDA. The ψ_{2000} field in the LDA shows a pair of high- and low-pressure cells whose centers are offset NW–SE diagonally. During the first month shown (upper row in Figure 7), these pressure cells remain relatively steady, changing neither their strength nor their orientation. During the second month (bottom row) the high-pressure cell moves southeastward displacing the low pressure in the LDA region. As the upper meander trough steepens to the northeast and the deep pressure cells shift to align their currents with the upper flow, parts of the northern front successively join the southern front as follows.

[34] 2. Waters at 400 dbar with temperatures between 4°C and 7°C switch between the fronts. On 18 June, the 6°C isotherm is clearly embedded within the northern branch; only waters colder than 4°C are associated with the southern front. Over the next month, the 4.5°–6°C waters progressively shift southward. By 20 July, the northern edge of the southern front is defined by the 6°C isotherm.

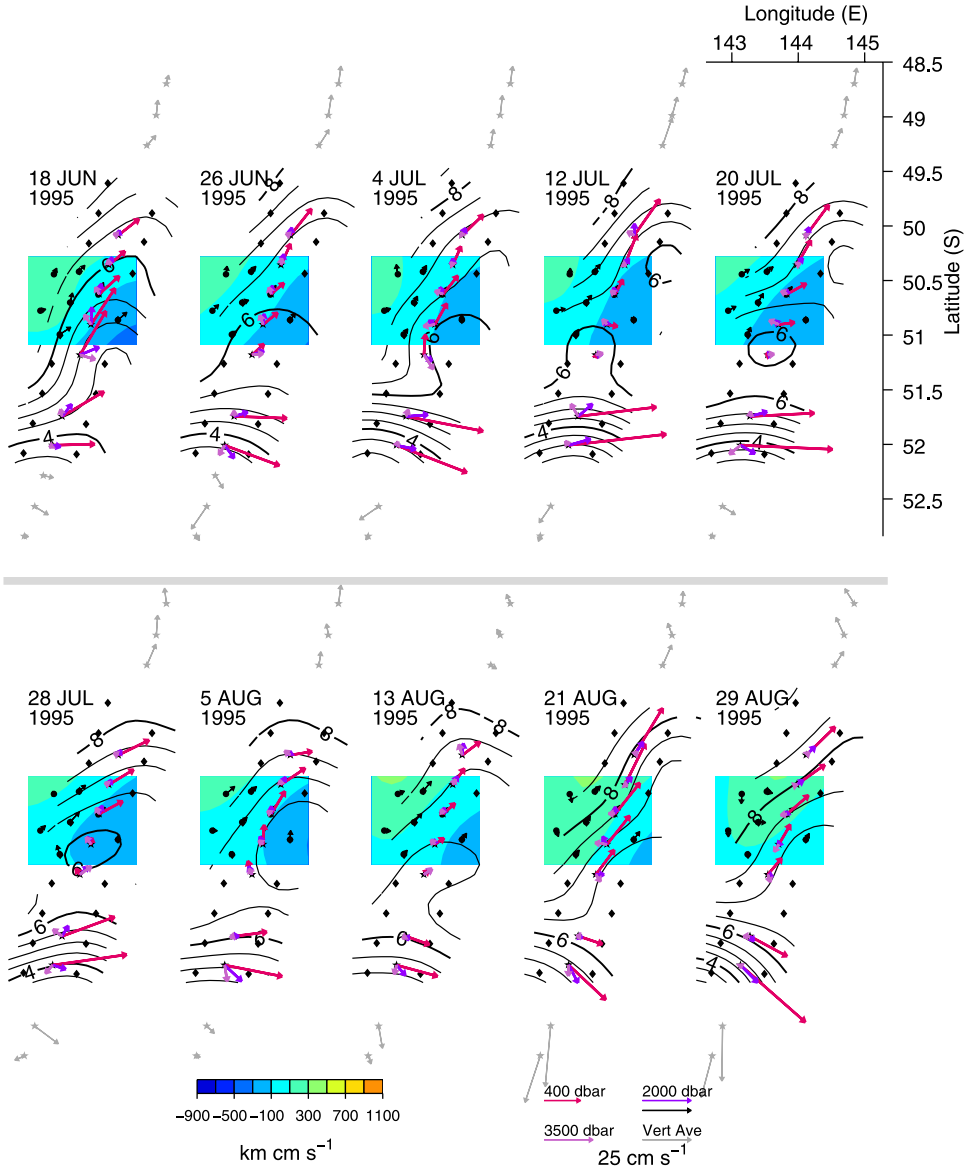

Figure 7. A 2.5-month period when two fronts were present as illustrated by T_{400}, ψ_{2000}, and velocity vector maps. Gray vectors show $\mathbf{V}_{VA}$ at HEFR sites north and south of the IES mapping region. Maps are shown at 8 day intervals.

[35] 3. On the four occasions when two fronts were present, waters colder than 4°C were always associated with the southern one. During this period, these waters flowed primarily eastward, although by late August, the currents shifted southeastward. While the southern front occasionally headed slightly north of east (such as on 28 July), the front itself never passed north of 51.5°S during any of the four periods.

[36] 4. The southern jet is always stronger than the northern jet. For most of the 2.5-month-long period shown in Figure 7, current speeds at 400 dbar near 52°S vary between 40–65 cm s^{-1}. Conversely, speeds rarely exceed 30 cm s^{-1} at the five sites in the northern front. While a portion of the northern front was outside the mapping array, the vertically averaged velocities ($\mathbf{V}_{VA}$) to the north of the IES mapping array show that the current does not strengthen; it either remains steady or weakens. From mid-June through early August, the $\mathbf{V}_{VA}$ at the southernmost HEFR sites are weaker and their headings differ, indicating that the southern front does not extend south of 52°S. By late August the southern front shifted south of 52°S outside the IES mapping array.

[37] 5. In both fronts, the currents often veer or back through ~90° with depth. For example, on 12 July, the currents at 400 dbar in the northern jet head generally to the northeast, while at 3500 dbar the flow direction is to the northwest. In the southern jet, the direction of the deep currents is more variable, fluctuating between northwest and southwest with 10–15-day periodicity. In both fronts the turning can be so great that u_{3500} is often westward.

5.2. Propagating Large-Amplitude Meander

[38] During the highly active second 6 months (November 1995 to May 1996), two large amplitude meanders propagated through the array. The sequence of T_{400} maps in

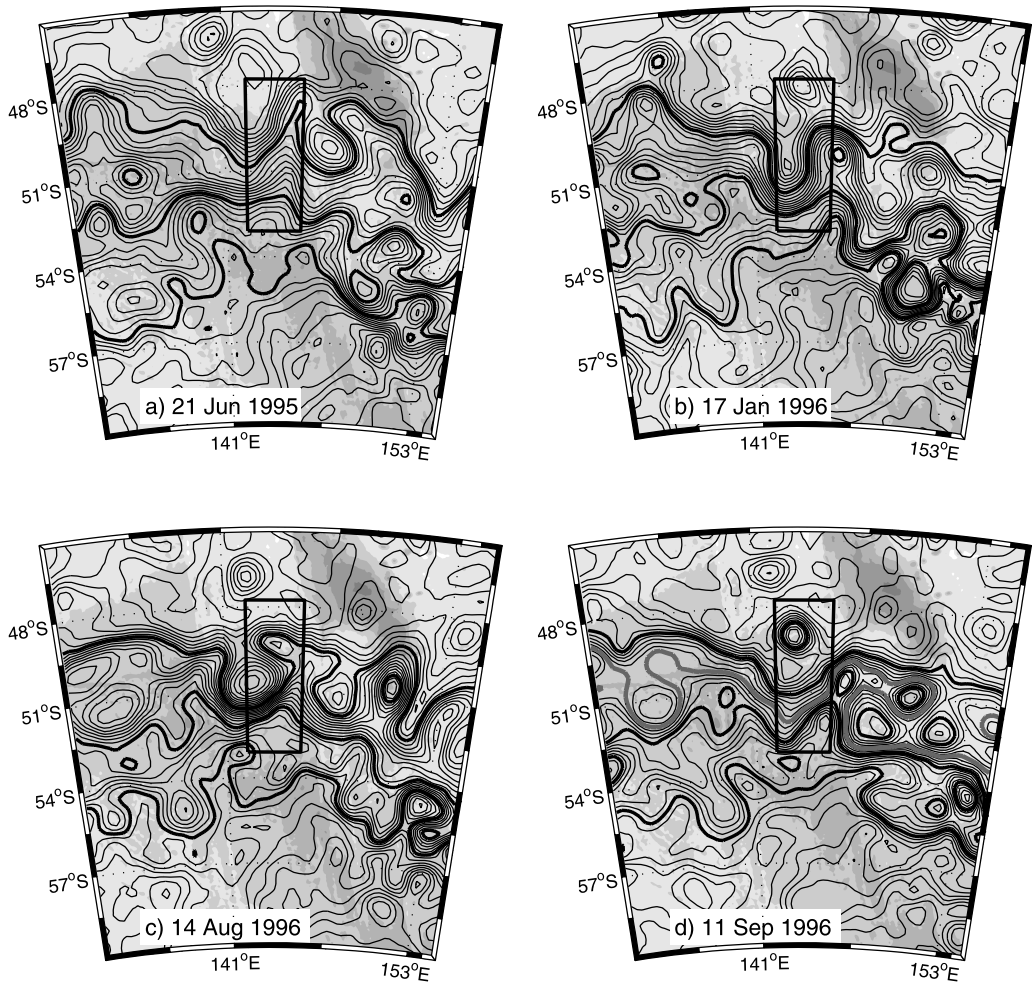

Figure 8. Sea surface height relative to 1500 m for (a) June 1995, (b) January 1996, (c) August 1996, and (d) September 1996. The bold contours (130, 85, and 55 cm) indicate the two branches of the SAF and the Polar Front, from north to south, respectively, identified within the SAFDE array. The thick gray contour in Figure 8d indicates the middle branch of the SAF. The contour interval is 5 cm. The boxed region encompasses all the SAFDE instrumentation as shown in Figure 1.

Figure 9 depicts the evolution of one of these meanders for a 70-day period beginning on 25 November 1995. Throughout this event the SAF existed as a single coherent front, identified by the strong gradient of the 4–8.5°C isotherms. When the daily frames are viewed as an animation (see auxiliary material[1]) the propagation and evolution of the set of meander crests and troughs is evident.

[39] On 25 November, the SAF flowed slightly south of east as a meander crest. A pool of water warmer than 8.5°C stretched northward from 51.25°S. This is the pycnostad of Subantarctic Mode Water that is typically found between the sea surface and 450–600 dbar. It is characterized by waters with potential densities ranging 26.8–26.9, which correspond to temperatures of 8°–9.5°C and salinities of 34.45–34.75 [*Rintoul and England*, 2002]. Circulation within this pool was cyclonic and the currents were vertically aligned all the way to the ocean bottom.

[40] In early December 1995, the SAF shifted northward along the western IES line as a large amplitude meander trough propagated into the array from the west. (Note that in the southern and northern hemispheres a trough shifts equatorward with cyclonic curvature.) By 5 December, the position of the SAF along the western IES line had translated more than 150 km north of its position on 25 November. The path of current, flowing nearly due south between the two lines of IESs, is the downstream flank of the meander trough.

[41] Over the next 10 days, the meander amplified and distorted. Although two fronts are present in the array on 10–20 December, they are clearly part of a single continuous front that has looped back on itself creating a 'folded' (reverse S) path. Using the 6°C isotherm to indicate the path, curvature (κ) of the path where the front loops back is estimated to be 0.02 km^{-1}. The velocities at 400 dbar ranged 85–98 cm s^{-1}, so $|\kappa v|$ is 15–18% of the planetary vorticity. Unlike on 25 November when the currents at all sites were vertically aligned, substantial turning with depth was observed between 10 and 15 December indicating vertical cross-frontal motions. For example, the currents near 50°–50.5°S turn clockwise with increasing height (backing) and the zonal component of flow at 3500 dbar is westward opposing that at 400 dbar. Bottom currents were very strong, reaching speeds of 20–30 cm s^{-1} at several sites.

Auxiliary materials are available in the HTML. doi:10.1029/2005JC002905.

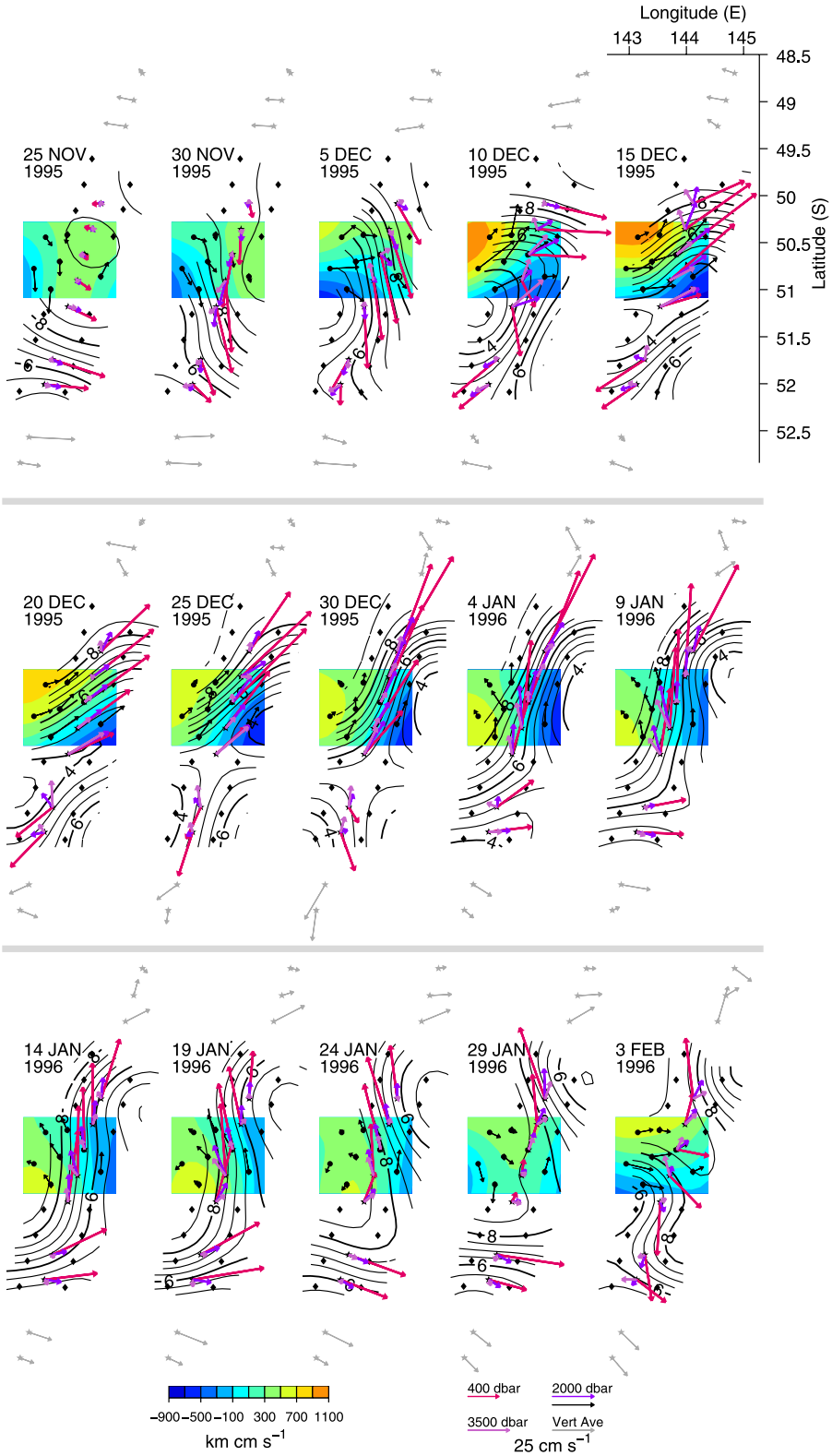

Figure 9. T_{400}, ψ_{2000}, and velocity vector maps during a 2-month period during the passage of a large-amplitude meander trough. Gray vectors show $\mathbf{V}_{VA}$ at HEFR sites north and south of the IES mapping region. Time interval is 5 days.

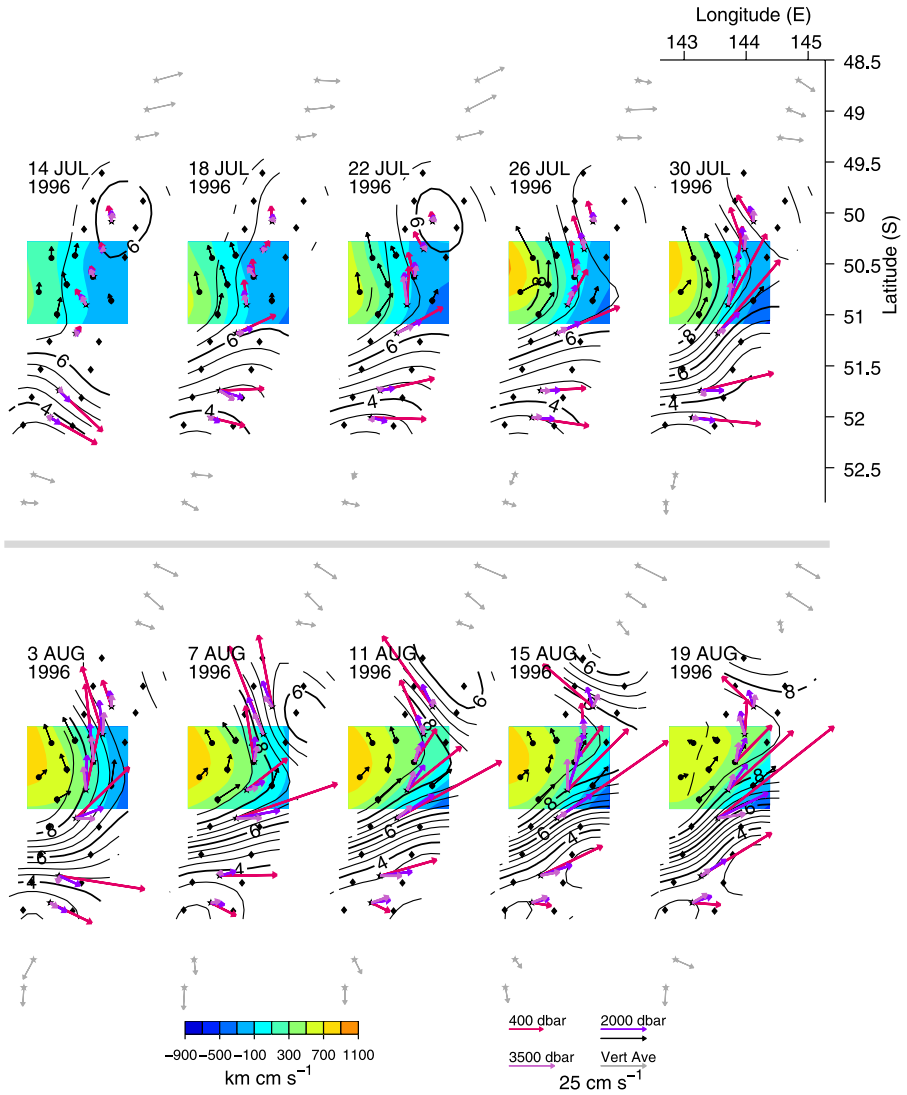

Figure 10. T_{400}, ψ_{2000}, and velocity vector maps during a 1-month period when the northern and southern fronts join to form a single front and a cold core eddy detaches from the SAF. Gray vectors show $\mathbf{V}_{VA}$ at HEFR sites north and south of the IES mapping region. Time interval is 4 days.

[42] Between 20 December 1995 and 4 January 1996 the meander trough propagated eastward, then stalled as it steepened. Simultaneously, the high- and low-pressure cells in the ψ_{2000} field shifted southward and northward, respectively, resulting in a zonal displacement of their centers. This ψ_{2000} development is consistent with stretching imposed by the lateral shift of the upper baroclinic structure. At the southern HEFR sites the $\mathbf{V}_{VA}$ vectors show that the SAF turned eastward. By 4 January, the downstream flank had propagated east of the array. The 6°C isotherm on 14 January traverses the full meridional extent of the array yielding a crest-to-trough amplitude of at least 250 km.

[43] The SSH field for 17 January 1996 (Figure 8b) shows two branches of the SAF merged into a single, broad front near 137°E. Lateral surface height gradients are intensified where the front undergoes strong meandering within the SAFDE array. The array spans the steep meander trough and the trailing steep meander crest. While the broad-scale development of this large amplitude meander was detected with the SSH maps, the detailed spatiotemporal evolution of the mesoscale features revealed in the daily synoptic maps was not captured and resolved by the altimeters.

[44] By late January, the SAF once again flowed eastward along the southern edge of the array as a meander crest. Altogether, a single combined SAF meandered through this developing crest-trough pair, lingering for nearly 2 months within the array (25 November 1995 to 29 January 1996).

5.3. Eddy Formation

[45] From mid-June to mid-July 1996, the southern branch of the SAF flowed along the southern portion of the array while the northern branch shifted equatorward such that it was north even of the northernmost IESs. Large eastward flowing $\mathbf{V}_{VA}$ vectors at the three northernmost HEFR sites confirm its location. Between the two jets, a large region (extending meridionally from 49.5°S to 51.5°S) was filled with 5.5°–6.5°C water with weak circulation and little vertical sheer. The T_{400} map for 14 July 1996 (Figure 10) is representative of this month-long period.

[46] Commencing 18 July, the stability of the split front configuration was disrupted and the two fronts rejoined and developed as follows. During 18–30 July, a meander crest in the northern front propagated from the west shifting the 6.5°–8°C waters southward. Additionally, a trough in the southern front (4°–6°C isotherms) approached from the west, and its flow within the array changed from ESE to NE. These developments moved the two branches close together along the western edge of the mapping region. By 30 July, a single front entered the IES array as part of a large meander crest. These features are also captured in SSH field for 14 August (Figure 8c). The deep anticyclone in the ψ_{2000} field intensified as the meander crest developed; the strong gradients between the developing cyclone and anticyclone produced northward currents in excess of 25 cm s^{-1} at 2000 dbar. The deep anticyclone was offset to the north of the T_{400} expression of the crest, but the array width was too narrow to resolve the along-stream alignment.

[47] As the deep anticyclone propagated eastward into the LDA (3–19 August 1996), the T_{400} front folded sharply back into an S path and the observed flow in the northern portion of the mapping array was to the northwest. The northern $\mathbf{V}_{VA}$ show that the flow turned eastward again near 48.5°–49°S. The S-shaped path in the SAFDE region is apparent in the SSH field (Figure 8c).

[48] The three northern $\mathbf{V}_{VA}$ vectors on 11–19 August 1996 suggest that a cold core eddy detached from the SAF. The longitude of separation is outside the array, but is estimated to be near 146°E. This longitude lies within the cold-core eddy generation region (144°–150°E) identified by *Morrow et al.* [2004]. Corroboration of the eddy's detachment is provided by *Sokolov and Rintoul* [2002]. Hydrographic data collected along the SR3 line during September 1996 exhibited weak doming of the isopycnals near 49°S, indicating that their survey had crossed the eastern flank of the eddy. They observed cyclonic flow throughout the upper 300 m with concurrent shipboard acoustic Doppler current measurements. Additionally, a strong eddy was apparent north of the SAF front and west of SR3 in the SSH field for 11 September 1996 shown in their paper (and also Figure 8d).

5.4. Propagating Small-Amplitude Meander

[49] *Sokolov and Rintoul* [2002] reported a third (or middle) branch of the SAF near 51.7°S during their September 1996 occupation of SR3. This third branch is commonly observed in satellite SSH fields farther west, between 130° and 137°E, but they identified it as a separate front in the SAFDE region in only one of six hydrographic sections along SR3. Figure 8d shows the SSH field for 11 September with the middle SAF branch emphasized. (Subtle SSH differences arising from the choice of referencing mean field can be assessed by comparing this map with that shown by *Sokolov and Rintoul* [2002] which is referenced to 2500 m.)

[50] *Sokolov and Rintoul* [2002] identified the location of the three branches of the SAF by determining local maxima in the temperature gradient for temperatures between 4° and 8°C using the hydrographic data along SR3. They found peak gradients at 50.9°, 51.7°, and 52.9°S corresponding to T_{400} ranges of 7°–9°C, 5°–6°C, and 3°–4°C, respectively. Their occupation of SR3 passed through the array on 10–13 September. Two fronts in close proximity are evident in the T_{400} maps for 10–14 September (middle row in Figure 11) as the strong thermal gradients between 6°–8.5°C and between 4.5°–5°C. The latitudes corresponding to these peak gradients are near 50.7°S and 51.9°S, in good agreement with those identified as the northern and middle SAF from the hydrography. The southern front identified with the station data flowed outside the IES mapping region during this time period, near where the southern most HEFR exhibited increased $\mathbf{V}_{VA}$.

[51] The interpretation of these lateral gradients as three distinct fronts becomes doubtful when a sequence of maps (Figure 11) produced from the moored data is examined. At the end of August 1996 the SAF flowed to the northeast as a single jet through the array. The lateral temperature gradients at 400 dbar across the front were strong and the corresponding velocities exceeded 60 cm s^{-1}. Between 4 and 14 September, the 5.5°–8°C isotherms shifted northward creating one front, while colder waters formed a second, but weaker, front at the southern end of the mapping array. Yet only a few days later (16 September) the 4°–8°C isotherms formed a single front which persisted until 26 September.

[52] This time sequence reveals that a small amplitude meander passed through the array at the time of the SR3 occupation. The absence of westward zonal flow at 400 dbar indicates that it is a meander, not an embedded eddy. The crest-to-trough amplitude estimated from the IESs is approximately 40 km and the eastward propagation speed is about 7 km d^{-1}. The spatiotemporal resolution in this set of maps indicates that the middle front identified by *Sokolov and Rintoul* [2002] along SR3 was an artifact of sampling a small, rapidly propagating meander on a single transect. This more complete evidence indicates that it was not a separated, continuous front during this time in the SAFDE region.

6. Discussion

[53] The short zonal extent of the array made it difficult to identify some features as meanders or eddies or varicose modes. While the satellite SSH maps provided a view of the fronts over a larger region, they did not adequately resolve the time development of the mesoscale features. Nevertheless, an overall summary of the events during the 2-year observations can be provided with good certainty regarding most aspects of the fronts in this region: About 10 small-amplitude meanders or eddies passed through the region. Four large meanders with crest-to-trough amplitudes of at least 250 km propagated eastward through the array and developed into convoluted structures. A ring-like eddy pinched off to the north of the SAF during the passage of one meander trough. On four occasions, the flow was divided into two jets that were separated zonally. These split front configurations persisted for 1–2 months after which meandering brought the fronts together again to form a single front. The propagation and evolution of these events may also be viewed in the provided animation of the daily frames.

[54] During the passage of the large-amplitude meanders, the isotherms typically used to identify the SAF (4°–8°C) formed a single, coherent front. Observed currents at

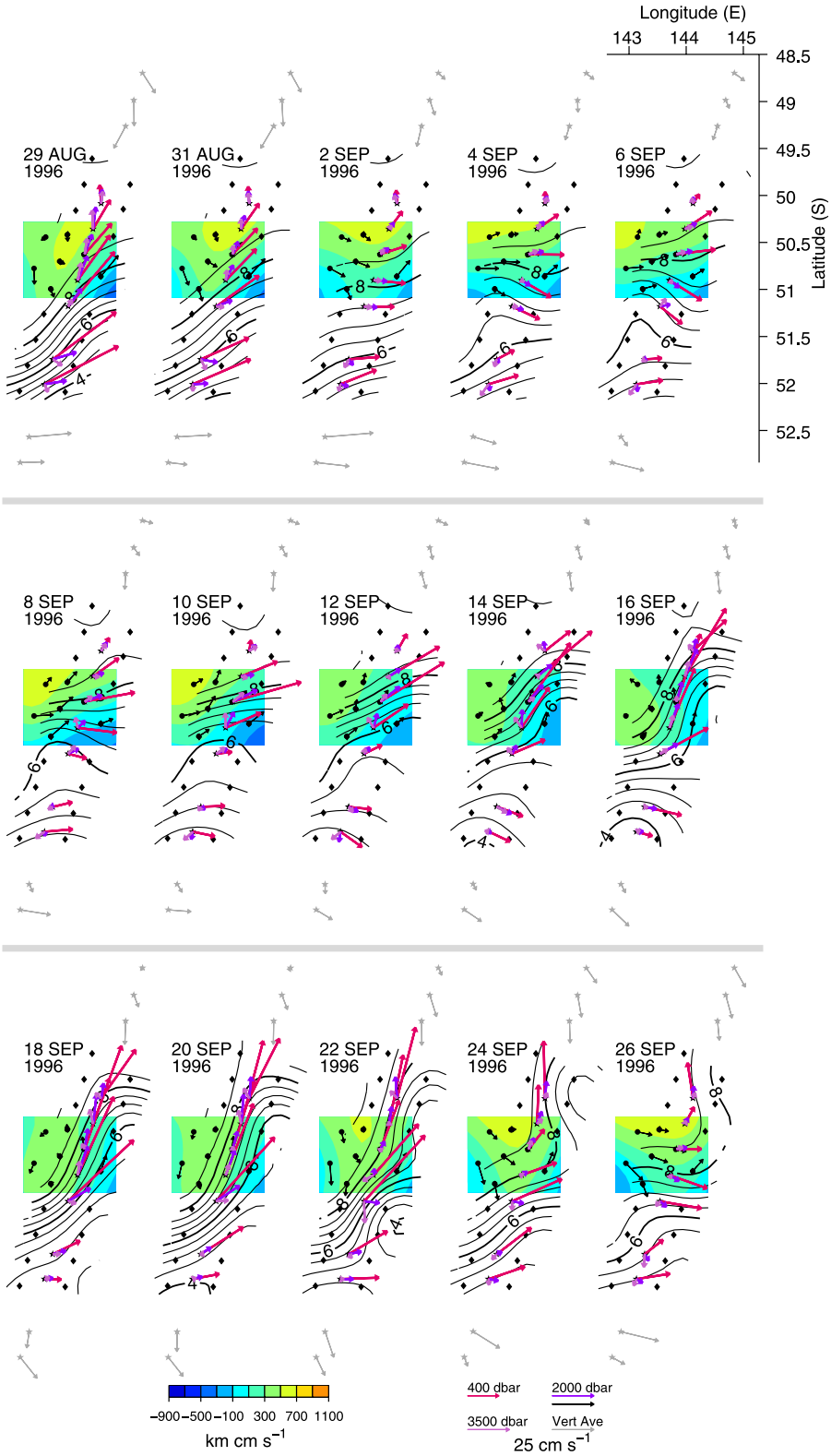

Figure 11. T_{400}, ψ_{2000}, and velocity vector maps during a 1-month period during the passage of a small-amplitude meander. Gray vectors show $\mathbf{V}_{VA}$ at HEFR sites north and south of the IES mapping region. Time interval is 2 days.

400 dbar reached speeds of 60–100 cm s^{-1}. Although the baroclinic structure extends to near bottom in the SAFDE region, significant turning of the currents with depth was observed during the passages of these meanders (Figures 9 and 10). This resembles the Gulf Stream where *Lindstrom and Watts* [1994] and *Lindstrom et al.* [1997] showed that deep barotropic flow crossing the upper front drives important cross-frontal exchanges. Every steep meander eventually

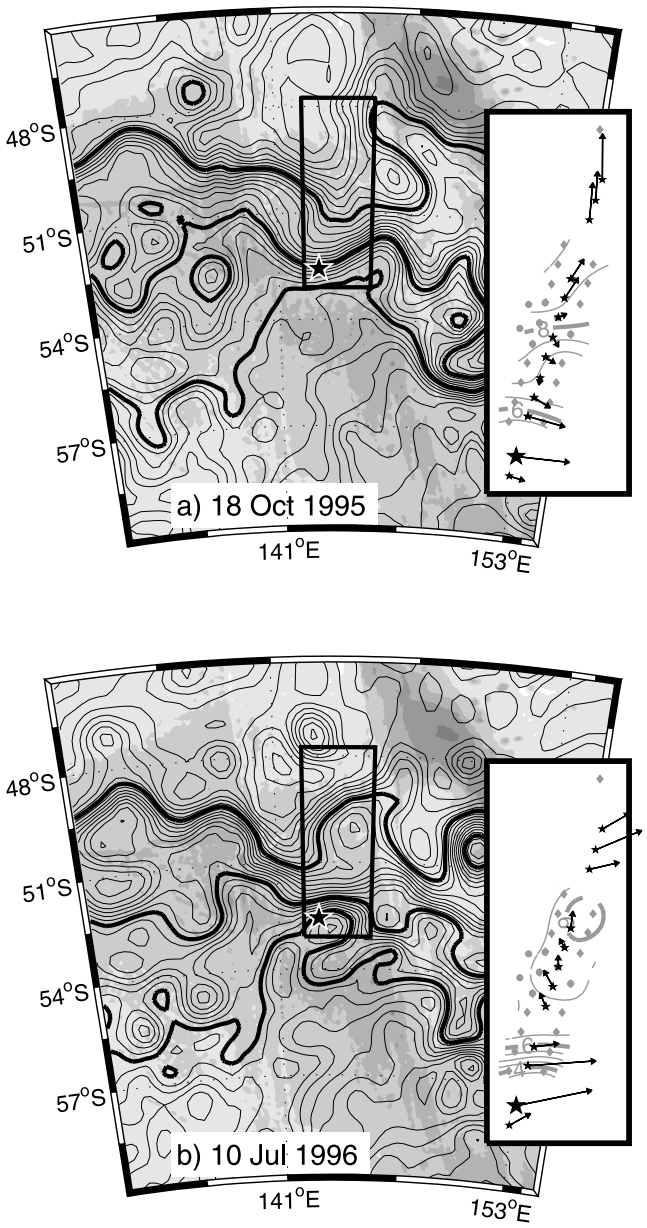

Figure 12. Same as in Figure 8 except for (a) October 1995 and (b) July 1996 when the northern branch of the Polar Front extended into the southern potion of the SAFDE array. The insets show the SAFDE data for the same date within the boxed region. Black vectors show $\mathbf{V}_{VA}$ at the HEFR sites. T_{400} fields are contoured in gray. HEFR 16 is marked by the large star in the SSH maps and insets.

folded back on itself forming an S-shaped (or reverse-S-shaped) front, but the direction of rotation varied with each event. Sometimes the axis of a crest or trough rotated to the ENE–WSW, at other times it rotated to the WNW–ESE. These meanders were so steep that they nearly stalled and took between 1–3 months to transit 55 km downstream through the mapping array.

[55] On other occasions for many weeks in a row, two fronts were observed in the array separated by a region with low thermal gradients. When two fronts were present, stronger velocities were observed within the southern one. Current speeds at 400 dbar were more than a factor of 2 stronger in the southern jet and correspondingly, the horizontal thermal gradients that form the southern front were sharper (e.g., Figure 7). Differences in the current strengths are readily apparent in the velocity time series in Figures 3a, 3b and 3c and the mean vectors shown in Figure 5 for the first 6 months of the deployment. The daily maps reveal that the southern front did not meander north of 51.5°S, so it was never sampled by the current meters in the LDA. Two velocity maxima were also observed by *Phillips and Rintoul* [2002] in geostrophic currents calculated from several CTD transects. Although they show higher mean velocities in the northern branch, peak geostrophic velocities in the southern front were higher on several of the individual sections [*Phillips and Rintoul*, 2002, Figure 13].

[56] Waters with temperatures warmer than 7°C at 400 dbar were found in the northern front and those colder than 4°C in the southern front. Waters with temperatures between 4°C and 7°C alternately associated with either front. These fronts agree well with the two branches of the SAF defined by *Sokolov and Rintoul* [2002]. They found that the northern SAF was usually located between 50° and 51°S. During this experiment, the mean location of the northern jet was found at the same range of latitudes. However, the daily maps show that the northern jet frequently shifted north of the IES mapping array and strong flows were observed at the northernmost HEFR sites. Thus it was common for the northern flow to shift as far north as 49°S. The mean location of the southern front during SAFDE was south of 51.5°S, which is in good agreement with the 52°–53°S location of the southern SAF reported by *Sokolov and Rintoul* [2002]. In contrast, *Gille*'s [1994] analysis of Geosat altimetry from 1986–1989 (using techniques that predated the finding of two SAF branches) reported the mean location of the Polar Front was at 52°S at this longitude.

[57] Is the southern front observed during SAFDE a branch of the SAF or does it merge with the Polar Front? *Belkin and Gordon* [1996] and *Rintoul et al.* [2001] state that the southern SAF and the northern branch of the PF occasionally merge to form a single front. The Polar Front is commonly identified by the northernmost extent of the subsurface temperature minimum cooler than 2°C near 200 m [*Belkin and Gordon*, 1996; *Sokolov and Rintoul*, 2002]. Maps of temperature at 200 dbar generated from the IESs reveal that waters as cold as 2°C did not penetrate as far north as the IES temperature mapping array. Yet in the mean the strongest $\mathbf{V}_{VA}$ currents in the southern portion of the array were observed at HEFR 16 at 52.6°S (10.0 cm s^{-1}). Mean $\mathbf{V}_{VA}$ currents at the neighboring sites were weaker, 9.3 cm s^{-1} at HEFR 14 and 7.3 cm s^{-1} at HEFR17. These velocity observations suggest that while the PF never reached as far north as the IES mapping array, it likely reached as far north as the two southernmost HEFRs. Additionally, *Rintoul et al.* [1997] observed the PF as far north as 52.6°S in a few of the hydrographic sections conducted between 1991 and 1994. To investigate this possibility, the SSH fields were examined for periods when strong $\mathbf{V}_{VA}$ occurred at the southernmost HEFR sites. Representative SSH maps (Figure 12) show two periods when the northern branch of the PF penetrated the southern edge of the SAFDE array and strong $\mathbf{V}_{VA}$ speeds were

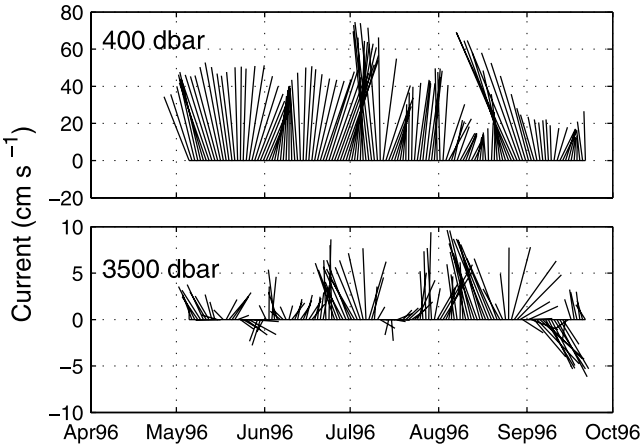

Figure 13. Currents at 400 and 3500 dbar at HEFR 14. Upward pointing arrows indicate eastward flow.

observed at HEFR 16. From early October to late November 1995, the PF skirted the array following a relatively straight path and the corresponding HEFR 16 and 17 currents flowed primarily eastward. In contrast, vigorous meandering during a two week period in July 1996 brought the northern PF as far north as HEFR 16 where the $\mathbf{V}_{VA}$ speed was 30 cm s^{-1}. In all, there were four periods (typically two weeks in duration) during the 2-year SAFDE field program when the northern PF reached as far north as 52.6°S, merging with the southern SAF front.

[58] The AUSSAF array of four current meter moorings deployed during 1993–1995 [*Phillips and Rintoul*, 2000] in the same locationas our LDA yielded many important results that can be clarified or enhanced with the SAFDE measurements. They discovered unexpected northeastward flow in the mean, evidence for a meander in the path of the SAF over the array. The mean fields from SAFDE show that a second front of eastward flow persisted south of the standing meander. This mean pattern is robust as it exists in both the 6-month means as well as the 2-year mean. However, the SAFDE measurements also reveal that the mean pattern can arise from two distinctive circumstances, either because two discrete fronts exist (as occurred during April through September 1995) or alternatively, as an artifact of a strongly meandering, single SAF front (as occurred during October 1995 through March 1996).

[59] The northern jet meanders more than the southern jet in the SAFDE region. For example, the first 7 months (and, to a lesser extent, the last 4 months) of the currents at HEFR 7 and 11 (Figures 3a, 3b and 3c) display weak variability compared with the rest of the time period. In contrast, the currents in the southern front (cf. HEFR 14) vary energetically throughout the time period. The AUSSAF mooring data [*Phillips and Rintoul*, 2000, 2002] from 1993 to 1995 also exhibited less variability during the first and last 100–150 days of the records. These observations suggest a quasi-biennial cycle in the variability of the northern SAF.

[60] *Lindstrom et al.* [1997] described the relationship between vertical velocity and the phasing of meanders for the Gulf Stream. They found that downwelling occurs entering meander troughs (what they termed "bcd" for backing, cold advection and downwelling) and upwelling occurs entering meander crests (termed "uvw" for upwelling, veering and warm advection). On the basis of measurements during isolated events, *Phillips and Rintoul* [2000] concluded that the relationship between vertical motion and meander phase determined by *Lindstrom et al.* [1997] for the Gulf Stream holds true for the SAF. Yet they found that this relationship did not hold true in the mean. However, they lacked measurements of the path, and so could not determine the location of the meander relative to the array. Furthermore, *Phillips and Rintoul* [2000] stated that "bcd" was observed only when the flow was heading to the northeast. The simultaneous observations of path and currents during SAFDE provide confirmation that the relationship between vertical motion and meander phase holds for the mean (Figure 5) as well as for individual events. The daily maps also reveal that "bcd" and "uvw" occur in the presence of strong abyssal circulations regardless of the flow direction of the SAF. For example, on 10–15 December 1995 (Figure 9), a deep cyclone/anticyclone pair intensified as a large-amplitude meander developed. The flow at 400 dbar is eastward at HEFR 8 and 9 and southward at sites HEFR 10 and 12. Nevertheless, the deep flow at all four of these locations crosses the baroclinic front at large angles, and through the upper layers of this flow entering the trough, the rotation in the vertical is consistent with "bcd".

[61] Several studies have stated that the zonal component of the bottom flow is eastward, aligned with that of the upper jet in an equivalent barotropic sense, both instantaneously [*Donohue et al.*, 2001] and in the mean [*Killworth*, 1992; *Gille*, 2003]. Even the synoptic mean absolute velocity profile averaged in stream coordinates by *Meinen et al.* [2003] from the SAFDE measurements supports this vertical alignment. The mapped fields shown here, however, indicate that this is an overly generalized view of the abyssal flow field. The maps illustrate numerous instances when the zonal flow directions of the upper and deep currents coincide, yet there are just as many examples when they do not. Deep cyclones and anticyclones propagate through the SAFDE array and the position of their centers relative to the upper flow determines the vertical alignment. Current vectors for the 400 and 3500 dbar levels at HEFR 14 illustrate how different the deep and upper currents can be (Figure 13). Three deep cyclonic eddies passed over the site at approximately 50 day intervals between May and October 1996. These eddies translated from west to east at 20–30 km d^{-1}. The deep currents rotate clockwise through all directions while the zonal component of the upper flow was always eastward.

[62] Several examples of closed eddies that are separated from the SAF exist in the ACC literature and in our observations. Satellite sea surface height maps (cf. Figure 8 and *Sokolov and Rintoul* [2002]) show eddy-like features in addition to multiple fronts in the region spanning Tasmania and Antarctica. Several eddies were observed by *Donohue et al.* [2001] near the SAF front in velocity-referenced hydrographic sections spanning the current across the Pacific Ocean. Current meters measured cyclonic flow in a cold core eddy that passed over the moorings on the Campbell Plateau south of New Zealand [*Stanton and Morris*, 2000]. Using altimetry and hydrographic data, *Morrow et al.* [2004] examined the propagation and vertical

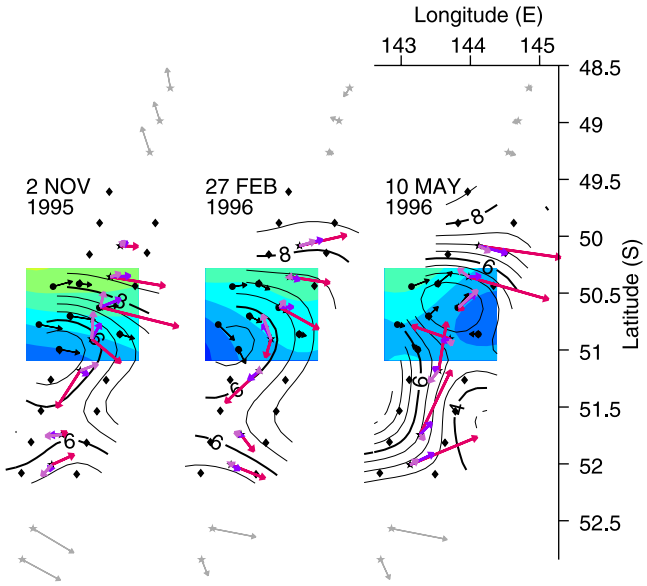

Figure 14. T_{400}, ψ_{2000}, and velocity vector maps illustrating three different cyclonic eddies embedded within the eastward flowing SAF. Gray vectors show $\mathbf{V}_{VA}$ at HEFR sites north and south of the IES mapping region.

structure of cold core eddies shed to the north of the SAF between 140°E and 150°E. During SAFDE, a cyclonic, cold core eddy detached on the northern side of the SAF front in late August 1996 (Figure 10). This eddy, with core temperatures below 6°C at 400 dbar and roughly 140 km in diameter, propagated away from the study region to the northwest. It may have been reabsorbed into the SAF during the passage of a large meander a few months later.

[63] Closed eddies also exist embedded within the SAF. In one instance, *Donohue et al.* [2001] observed an embedded cyclonic eddy which divided the strong eastward flow of the jet into two regions. During SAFDE, similarly embedded eddies propagated from west to east through the array. Three of these are pictured in Figure 14. The eddies were about 100 km in diameter and their centers transited the array between latitudes 50.5°–51.25°S (near the southern edge of the LDA). Currents with swirl speeds of 30 cm s^{-1} at 400 dbar rotated cyclonically around cold cores of about 5°C.

7. Summary

[64] The SAFDE array, centered near 51°S, 143.5°E, provides a unique view of the Subantarctic Front south of Tasmania. Although the zonal extent was only 55 km, the array extended nearly 450 km meridionally. This is the only moored array in the Southern Ocean to use long-duration, spatially coherent current and temperature records having mapping capabilities with mesoscale resolution. This experiment yielded daily maps of temperature and geostrophic velocity at a suite of depth levels for April 1995 through March 1997. Profiles of absolute velocity were obtained at seven sites by combining HEFR and IES measurements [*Meinen et al.*, 2002].

[65] The daily maps show that the SAF often flowed as a strong single jet. The lateral temperature gradients of the front at 400 dbar were sharp (changing from 4°C to 8°C over a 75 km distance) and the corresponding velocities were swift (>140 cm s^{-1}). During these intervals the SAF tended to exhibit vigorous meandering. Large-amplitude meanders with crest-to-trough amplitudes of about 250 km stalled and developed within the array. Propagating meanders had periods of 20–70 days, wavelengths of 240–420 km, and phase speeds of 12 km d^{-1} to 6 km d^{-1}. Deep eddies consistently led the upper meanders, exhibiting the vertical phase tilt characteristic of baroclinic instability [*Lindstrom et al.*, 1997]. These features jointly propagated eastward.

[66] At times, the SAF was also observed as two distinct jets, which typically persisted separately for 1–2 months. The northern jet generally flowed to the northeast, while the southern jet flowed eastward. The currents in the southern branch were stronger than those in the northern branch by nearly a factor of 2. Rarely, the synoptic SAF also spread its lateral temperature gradient weakly across a broad baroclinic zone stretching about 200 km wide.

[67] The large-scale satellite SSH fields, while not fully resolving the mesoscale features of the SAF region, suggest that the SAF often exists as two meridionally separated zonal jets upstream of the SAFDE array (west of 140°). Meandering, and probably topographic influences, move these fronts closer together between 137°E and the SAFDE array. At times during the experiment these fronts remained separate and passed through the SAFDE array as two distinct jets. At other times, when the SSH fields showed that both fronts were meandering vigorously upstream of the SAFDE array, the two fronts merged to form a single jet within the SAFDE domain, "zippering" the front together from west to east. The SSH maps also suggest that the merged branches often reseparate and remerge again farther downstream. All four clear cases of separation that occurred during these 2 years within the SAFDE domain appeared to grow from the southeastern edge of the array because of interactions with downstream eddies which "unzippered" the front from east to west. The mesoscale-resolving maps from SAFDE trace the development of these features over time, revealing processes that are not apparent in hydrographic or satellite measurements.

[68] Last, although the SAF baroclinic front reaches from the sea surface to the seafloor, the measured currents reveal that strong eddies exist at times throughout the lower water column, resulting in deep flows with substantial cross-front components (even in the 2-year mean), and at times counter to the surface flow.

[69] **Acknowledgments.** The Sub-Antarctic Flux and Dynamics Experiment was designed by Alan Chave (WHOI), Jean Filloux (SIO), Doug Luther (UH), Jim Richman (OSU), and Randy Watts (URI) in collaboration with John Church and Steve Rintoul (CSIRO) after discussions with Eric Lindstrom in 1990. We would like to thank Steve Rintoul, Alan Chave, and the anonymous reviewers for suggestions that improved an earlier draft of the manuscript. We wish to thank the captain and crew of the R/V *Melville* for their assistance at sea and the technical groups at URI and WHOI for their preparation of the IESs and HEFRs, at Scripps for their work on the HEFRs, and at OSU and CSIRO for their preparation of the current meters. SAFDE was funded in the United States under NSF grants OCE92-04063, OCE92-04113, OCE92-04041, OCE99-12110, OCE99-12320, and OCE99-11974.

References

Belkin, I. M., and A. L. Gordon (1996), Southern Ocean fronts from the Greenwich meridian to Tasmania, *J. Geophys. Res.*, *101*, 3675–3696.

Best, S. E., V. O. Ivchenko, K. J. Richards, R. D. Smith, and R. C. Malone (1999), Eddies in numerical models of the Antarctic Circumpolar Current and their influence on the mean flow, *J. Phys. Oceanogr.*, *29*, 328–350.

Bretherton, F. P., R. E. Davis, and C. B. Fandry (1976), A technique for objective analysis and design of oceanographic experiments applied to MODE-73, *Deep Sea Res.*, *23*, 559–582.

Bryden, H. L., and R. A. Heath (1985), Energetic eddies at the northern edge of the Antarctic Circumpolar Current in the southwest Pacific, *Prog. Oceanogr.*, *14*, 65–87.

Chave, A. D., and D. S. Luther (1990), Low-frequency, motionally induced electromagnetic fields in the ocean: 1. Theory, *J. Geophys. Res.*, *95*, 7185–7200.

Chave, A. D., D. S. Luther, and C. S. Meinen (2004), Correction of motional electric field measurements for galvanic distortion, *J. Atmos. Oceanic Technol.*, *21*, 317–330.

Chelton, D. B., M. G. Schlax, D. L. Witter, and J. G. Richman (1990), Geosat altimeter observations of the surface circulation of the Southern Ocean, *J. Geophys. Res.*, *95*, 17,877–17,903.

Donohue, K. A., E. Firing, and S. Chen (2001), Absolute geostrophic velocity within the Subantarctic Front in the Pacific Ocean, *J. Geophys. Res.*, *106*, 19,869–19,882.

Gille, S. T. (1994), Mean sea surface height of the Antarctic Circumpolar Current from Geosat data: Method and application, *J. Geophys. Res.*, *99*, 18,255–18,273.

Gille, S. T. (2003), Float observations of the Southern Ocean. Part I: Estimating mean fields, bottom velocities, and topographic steering, *J. Phys. Oceanogr.*, *33*, 1167–1181.

He, Y., D. R. Watts, and K. L. Tracey (1998), Determining geostrophic velocity shear profiles with inverted echo sounders, *J. Geophys. Res.*, *103*, 5607–5622.

Johnson, M. G. (1989), Southern Ocean surface characteristics from FGGE buoys, *J. Phys. Oceanogr.*, *19*, 696–705.

Killworth, P. D. (1992), An equivalent-barotropic mode in the Fine Resolution Antarctic Model, *J. Phys. Oceanogr.*, *22*, 1379–1387.

Kim, H.-S., and D. R. Watts (1994), An observational streamfunction in the Gulf Stream, *J. Phys. Oceanogr.*, *24*, 2639–2657.

Lindstrom, S. S., and D. R. Watts (1994), Vertical motion in the Gulf Stream near 68°W, *J. Phys. Oceanogr.*, *24*, 2321–2333.

Lindstrom, S. S., X. Qian, and D. R. Watts (1997), Vertical motion in the Gulf Stream and its relation to meanders, *J. Geophys. Res.*, *102*, 8485–8503.

Luther, D. S., J. H. Filloux, and A. D. Chave (1991), Low-frequency, motionally induced electromagnetic fields in the ocean: 2. Electric field and Eulerian current comparison, *J. Geophys. Res.*, *96*, 12,797–12,814.

Luther, D. S., A. D. Chave, J. A. Church, J. H. Filloux, J. G. Richman, S. R. Rintoul, and D. R. Watts (1997), The Sub-Antarctic Flux and Dynamics Experiment (SAFDE), *Int. WOCE Newsl.*, *29*, 32–35.

Meinen, C. S., and D. R. Watts (2000), Vertical structure and transport on a transect across the North Atlantic Current near 42°N: Time series and mean, *J. Geophys. Res.*, *105*, 21,869–21,891.

Meinen, C. S., D. S. Luther, D. R. Watts, K. L. Tracey, A. D. Chave, and J. Richman (2002), Combining inverted echo sounder and horizontal electric field recorder measurements to obtain absolute velocity profiles, *J. Atmos. Oceanic Technol.*, *19*, 1653–1664.

Meinen, C. S., D. S. Luther, D. R. Watts, A. D. Chave, and K. L. Tracey (2003), Mean stream-coordinates structure of the Subantarctic Front: Temperature, salinity, and absolute velocity, *J. Geophys. Res.*, *108*(C8), 3263, doi:10.1029/2002JC001545.

Mestas-Nunez, A. M., D. B. Chelton, and R. A. de Szoeke (1992), Evidence of time-dependent Sverdrup circulation in the South Pacific from Seasat scatterometer and altimeter, *J. Phys. Oceanogr.*, *22*, 934–943.

Morrow, R., R. Coleman, J. Church, and D. Chelton (1994), Surface eddy momentum flux and velocity variances in the Southern Ocean from Geosat altimetry, *J. Phys. Oceangr.*, *24*, 2050–2071.

Morrow, R., J.-R. Donguy, A. Chaigneau, and S. R. Rintoul (2004), Cold-core anomalies at the subantarctic front south of Tasmania, *Deep Sea Res., Part I*, *51*, 1417–1440.

Olbers, D., V. Gouretski, G. Seiss, and J. Schröter (1992), *Hydrographic atlas of the Southern Ocean*, Alfred Wegner-Inst. für Polar- und Meeresforchung, Bremerhaven, Germany.

Orsi, A. H., T. W. Whitworth III, and W. D. Nowlin Jr. (1995), On the meridional extent and fronts of the Antarctic Circumpolar Current, *Deep Sea Res., Part I*, *42*, 641–673.

Park, Y.-H., and L. Gamberoni (1995), Large-scale circulation and its variability in the South Indian Ocean from TOPEX/Poseidon altimetry, *J. Geophys. Res.*, *100*, 24,911–24,929.

Patterson, S. L. (1985), Surface circulation and kinetic energy distribution in the Southern Hemisphere ocean from FGGE drifting buoys, *J. Phys. Oceanogr.*, *15*, 865–884.

Phillips, H. E., and S. R. Rintoul (2000), Eddy variability and energetics from direct current measurements in the Antarctic Circumpolar Current south of Australia, *J. Phys. Oceanogr.*, *30*, 3050–3076.

Phillips, H. E., and S. R. Rintoul (2002), A mean synoptic view of the Subantarctic Front south of Australia, *J. Phys.Oceanogr.*, *32*, 1536–1553.

Reid, J. (1997), On the total geostrophic circulation of the Pacific Ocean: Flow patterns, tracers, and transports, *Prog. Oceanogr.*, *39*, 263–352.

Rintoul, S. R., and J. L. Bullister (1999), A late winter hydrographic section from Tasmania to Antarctica, *Deep Sea Res., Part I*, *46*, 1417–1454.

Rintoul, S. R., and M. H. England (2002), Ekman transport dominates local air-sea fluxes in driving variability of Subantarctic Mode Water, *J. Phys. Oceanogr.*, *32*, 1308–1321.

Rintoul, S. R., and S. Sokolov (2001), Baroclinic transport variability of the Antarctic Circumpolar Current south of Australia (WOCE repeat section SR3), *J. Geophys. Res.*, *106*, 2795–2814.

Rintoul, S. R., J. R. Donguy, and D. H. Roemmich (1997), Seasonal evolution of upper ocean thermal structure between Tasmania and Australia, *Deep Sea Res., Part I*, *44*, 1185–1202.

Rintoul, S. R., C. W. Hughes, and D. Olbers (2001), The Antarctic circumpolar current system, in *Ocean Circulation and Climate: Observing and Modelling the Global Ocean*, edited by G. Siedler, J. Church, and J. Gould, pp. 271–302, Elsevier, New York.

Rio, M.-H., and F. Hernandez (2004), A mean dynamic topography computed over the world ocean from altimetry, in situ measurements, and a geoid model, *J. Geophys. Res.*, *109*, C12032, doi:10.1029/2003JC002226.

Sanford, T. B. (1971), Motionally-induced electric and magnetic fields in the sea, *J. Geophys. Res.*, *76*, 3476–3492.

Savidge, D. K., and J. M. Bane (1999), Cyclogenesis in the deep ocean beneath the Gulf Stream: 1. Description, *J. Geophys. Res.*, *104*, 18,111–18,126.

Sciremammano, F., Jr., R. D. Pillsbury, W. D. Nowlin Jr., and T. Whitworth (1980), Spatial scales of temperature and flow in Drake Passage, *J. Geophys. Res.*, *85*, 4015–4028.

Shay, T. J., J. M. Bane, D. R. Watts, and K. L. Tracey (1995), Gulf Stream flow field and events near 68°W, *J. Geophys. Res.*, *100*, 22,565–22,589.

Smith, W. H. F., and D. T. Sandwell (1997), Global seafloor topography from satellite altimetry and ship depth soundings, *Science*, *277*, 1957–1962.

Sokolov, S., and S. R. Rintoul (2002), Structure of Southern Ocean fronts at 140°E, *J. Mar. Syst.*, *37*, 151–184.

Stanton, B., and M. Morris (2000), A month in the life of a subantarctic eddy, *Water Atmos.*, *8*, 19–20.

Tracey, K. L., S. D. Howden, and D. R. Watts (1997), IES calibration and mapping procedures, *J. Atmos. Oceanic Technol.*, *14*, 1483–1493.

Watts, D. R., K. L. Tracey, J. M. Bane, and T. J. Shay (1995), Gulf Stream path and thermocline structure near 74°W and 68°W, *J. Geophys. Res.*, *100*, 18,291–18,312.

Watts, D. R., C. Sun, and S. Rintoul (2001), A two-dimensional gravest empirical mode determined from hydrographic observations in the Subantarctic Front, *J. Phys. Oceanogr.*, *31*, 2186–2209.

Whitworth, T., III, and W. D. Nowlin Jr. (1987), Water masses and currents of the Southern Ocean at the Greenwich Meridian, *J. Geophys. Res.*, *92*, 6462–6476.

D. S. Luther, School of Ocean and Earth Science and Technology, Department of Oceanography, University of Hawai'i at Manoa, Honolulu, Hawaii, USA.

C. S. Meinen, Atlantic Oceanographic and Meteorological Laboratory, NOAA, Miami, Florida, USA.

K. L. Tracey and D. R. Watts, Graduate School of Oceanography, University of Rhode Island, South Ferry Road, Narragansett, RI 02882, USA. (ktracey@gso.uri.edu)